Arabian Journal of Geosciences (2021) 14: 1180
https://doi.org/10.1007/s12517-021-07559-5

ORIGINAL PAPER

Magnetite coated sand adsorbent for Cr(VI) removal from synthetic and pharmaceutical wastewater: adsorption isotherms and kinetics

Sahil Lakhanpal[1] · Anirban Dhulia[1] · Rajiv Ganguly[1]

Received: 3 January 2021 / Accepted: 8 June 2021 / Published online: 15 June 2021

Abstract

The present study analyzed the removal efficiency of Cr(VI) from synthetic and pharmaceutical wastewater streams using an adsorption technique by magnetite coated sand. In this context, batch experiments were performed using synthetic and pharmaceutical wastewater to analyze the influence of contact time and adsorbent dose on the removal efficiency of Cr(VI) in two different phases. Magnetite nanoparticles (Fe_3O_4) coated sand adsorbent was prepared by the coprecipitation method. The performances of the two batch reactors treating synthetic and pharmaceutical wastewater were compared to analyze the influence of contact time and adsorbent dose on Cr(VI) removal efficiency. In particular, different conditions of contact time and adsorbate concentration on the sorption process were studied. The adsorbent materials were further characterized by field emission scanning electron microscopy (FESEM), and the analysis of the Cr(VI) was analyzed using an inductively coupled plasma mass spectrometer (ICP-MS). Results obtained from the first phase of the study showed that for initial concentrations of 1 mg/L for both synthetic and pharmaceutical wastes, the remaining concentrations were determined to be 0.022 and 0.029 mg/L, respectively. The kinetic adsorption isotherms models have shown that the adsorbent follows the pseudo-second-order kinetic model. The isotherms were well fitted with Langmuir and Redlich–Peterson model, indicating monolayer adsorption of hexavalent Cr on the magnetite coated sand surface. However, the presence of other adsorbates in pharmaceutical wastewater influences the removal efficiency of Cr(VI) minutely. It can be inferred from the study that the adsorbent can be used for heavy metal treatment in a cost-effective manner since the magnetite is coated on the sand; it eliminates the problem of extraction of nanoparticles from treated wastewater and can be removed by a simple filtration process.

Keywords Cr(VI) removal · Magnetite nanoparticles · Pharmaceutical wastewater · Adsorption isotherm · Sand

Introduction

Heavy metals have always been an important environmental concern due to their carcinogenic nature and their ability in influencing human health in very small doses (Singh and Kalamdhad 2011; Tchounwou et al. 2012; Jaishankar et al. 2014; Ali et al. 2019; Sall et al. 2020). In particular, the major heavy metals of concern to human health and the surrounding environment are As, Pb, Hg, Cr, Se, Cd, V, Zn, and Co (Izuru et al. 1976; Jaishankar et al. 2014; Mishra et al. 2019; Tang et al. 2019; Sall et al. 2020). With increased urbanization and globalization, industries have been at the forefront of all anthropogenic sources leading to increased production of such heavy metals leading to their increased deposits in water bodies and sediments. Additionally, heavy metals are difficult to treat by biological methods since they are toxic to the bacterial pathogen leading to its continuous bioaccumulation and thereby needing continuous monitoring of such contaminated sources.

In the aforementioned context, Cr is considered as one of the most toxic elements present in the environment lying in group 6 and period 4 of the periodic table. The metal exists in two ionic states including trivalent Cr(III) and hexavalent Cr(VI) forms. Cr(VI) is both highly toxic and carcinogenic. In principle, Cr(VI) occurs as effluent from different industries including electroplating, pharmaceutical, refineries, and

Responsible Editor: Amjad Kallel

✉ Rajiv Ganguly
rajiv.ganguly@juit.ac.in

[1] Department of Civil Engineering, Jaypee University of Information Technology, District Solan, Waknaghat, Himachal Pradesh 173234, India

leather industry (Saha et al. 2011). The disposal regulations for inland surface water in India limit the concentrations of Cr(VI) and total Cr to 0.1mg/L and 2 mg/L, respectively, for inland surface water (CPCB 2017). Human exposure to Cr often leads to lung including nasal and sinus cancers, liver and kidney damage, skin lesions and abrasions, ulcers, and damage to eyes (Jaishankar et al. 2014; Sall et al. 2020). Hence, it needs to be treated to control human exposures.

In the previous context, there exist different methods for the removal of heavy metals from the wastewater stream. One of the most commonly used methods for the removal of heavy metals is the adsorption process. It is essentially a surface phenomenon, and the main principle of the process is an interphase accumulation of a substance at the surface of the adsorbent (Peng and Guo 2020; Kango and Kumar 2016). The process occurs between any two physical states including liquid–liquid, liquid–solid, or gas–liquid interphase.

In recent years, several studies have been conducted on magnetite adsorbents for the removal of Cr(VI) ions from the wastewater stream. Magnetite nanoparticles, maghemite nanoparticles, and mixtures of the previous two nanoparticles have been extensively studied for Cr(VI) removal. The efficiency and removal mechanism of Ni(II), Cu(II), and Cr(VI) from industrial wastewater was studied using maghemite nanoparticles where adsorption equilibrium for all the heavy metals was achieved within 10 min (Hu et al. 2006). The adsorption mechanism for Cr(VI) and Cu(II) was due to the combined effect of electrostatic attraction and ion exchange whereas, the Ni(II) adsorption was a result of electrostatic attraction only. In another reported study, the Cr(VI) adsorption capacity of maghemite nanoparticles was studied with carbon and clay adsorbents (Hu et al. 2005), and the study reported that at pH 2.5, 19.2 mg/g adsorption capacity was observed and was independent of initial Cr concentration. Adsorption equilibrium was achieved at 15 min. The adsorption capacity using carbon and clay was reported to be 15.47 mg/g and 11.55 mg/g, respectively (Hu et al. 2005). Several studies have also been conducted to investigate the removal of aqueous Cr(VI) using magnetite nanoparticles with or without functionalization agents. The investigation of the adsorption mechanism of coexisting Cr(VI) and Cu(II) in the water system using series of NH_2-functionalized nano-magnetic polymer adsorbents (NH_2–NMPs) coupled with different multi-amino groups was used (Shen et al. 2012). In another study, diatomite supported and unsupported magnetite nanocomposite was used as the adsorbent for Cr(VI) removal from aqueous solution, and a better adsorption capacity was achieved for the diatomite supported magnetite than the unsupported magnetite (Yuan et al. 2010). Further, organic iron-based composites, synthesized and immobilized by natural dried willow leaves, were used to investigate the removal of Cr(VI) from an aqueous solution (Yao et al. 2020). In a different reported study, magnetic biochar with different species of iron oxides (Fe_3O_4, Fe_2O_3, and FeO) was synthesized and studied for Cr(VI) removal (Yi et al. 2020). The maximum adsorption capacity of Cr(VI) by magnetic biochar was determined to be 71.04 mg/g of adsorbent used. The adsorption mechanism analysis identified that the Cr(VI) removal was due to the combined effect of electrostatic adsorption (surface electrostatic attraction and ion exchange), reduction, and complex formation techniques. Ullah et al. (2020) used synthesized magnetic max phase (MNPs- Ti_3AlC_2) and magnetic iron oxide for the removal of Cr(VI) ions from the tannery wastewater. The removal efficiency of Cr(VI) was recorded to be 99% at pH 3 with an adsorbent dose of 100 mg with an initial concentration of 1640 mg/L. The adsorption of Cr(VI) over MNPs- Ti_3AlC_2 was attributed to pseudo-second-order and endothermic processes. Arsenic (As) and Cr removal by maghemite and magnetite nanoparticles was studied, and the adsorption capacity of Cr was found to be 2.4 mg/g with an initial Cr(VI) concentration of 1 mg/L and 3.69 mg/g for As(III) and 3.71 mg/g for As(V) at pH 2.0. It was also observed that the presence of other ions in the water influence As and Cr adsorption, and the removal of arsenic is more favorable than the removal of chromium with maghemite–magnetite nanoparticles (Chowdhury and Yanful 2010). In another study, magnetite coated sand particles were used as an adsorbent for As(III) removal from synthetic wastewater (Kango and Kumar 2016).

As observed from the aforementioned studies, the magnetite–maghemite nanoparticles–based adsorption technique is well suited for the removal of heavy metals including Cr(VI). However, in all of the reported studies discussed in the previous paragraph, an external magnetic field was used to separate the magnetite nanoparticles from the water after treatment which in turn can induce additional waste generation (Dave and Chopda 2014; Ali et al. 2016a). The use of filter cartridges could be an alternative and effective method to overcome the application of an external magnetic field for the separation of magnetite nanoparticles from the wastewater stream.

The present study utilizes a magnetite nanoparticles–based adsorbent for removal of Cr(VI) obtained from the preparation of synthetic wastewater and was further utilized for removal of Cr(VI) from the pharmaceutical industry effluent. Batch experiments were performed to investigate the effect of contact time, adsorbent dose, and initial Cr(VI) concentration on the removal efficiency of Cr(VI). The study also presents two and three parameter-based adsorption isotherms to determine the efficiency of the process. Additionally, in the present study, we have utilized magnetite coated sand particles which itself acts as a filter cartridge medium as a result of which no external magnetic field is needed for the separation of the adsorbent thereby making the process highly cost-effective.

Materials and methods

Preparation of synthetic sample

The chemical solutions were prepared in Milli-Q water (BiocellMilli-Q Millipore, Elix). The chemicals used in the preparation of the synthetic sample were obtained from Sigma-Aldrich which were of analytical grade and hence were used without any additional purification. The Cr(VI) stock solution (500 mg/L) of the synthetic wastewater was prepared by dissolving a known amount of Cr sulfate, $Cr_2(SO_4)_3$ in Milli-Q water. The chromium(III) sulfate in the presence of alkaline medium (0.1 mol/L NaOH) leads to the formation of chromium hydroxide (Cr(III)) which further in the presence of H_2O_2 (10%) gets oxidized to chromate (Cr(VI)). This is the reaction mechanism that is followed for converting Cr(III) to Cr(VI) using chromium(III) sulfate. The pH of the stock solution was adjusted using standard acid and base solutions using 0.1 M HNO_3 and 0.1 M NaOH concentrations. Hence, the prepared synthetic wastewater contained Cr(VI) ions only and which were utilized for the study. Batch adsorption tests were carried out by diluting Cr(VI) stock solution into the desired initial concentration.

Collection of pharmaceutical wastewater

The pharmaceutical wastewater was taken from a working pharmaceutical industry. Samples were taken from the primary sedimentation tank outlet of the pharmaceutical industry. The wastewater was transported to the lab in PVC bottles after collection on the same day and was immediately stored at 4°C. The samples were analyzed using an inductively coupled plasma mass spectrometer (ICP-MS) to determine the Cr(VI) concentration.

Coating of magnetite nanoparticles on the sand surface

The Fe_3O_4 nanoparticles were synthesized using ferric chloride hexahydrate ($FeCl_3.6H_2O$), ferrous chloride ($FeCl_2$), and ammonium hydroxide (NH_4OH). The substrate sand was collected from the Beas River in Mandi district, Himachal Pradesh, India. Magnetite nanoparticles coated sand was prepared using the procedure of iron–chitosan coating on the sand (Gupta et al. 2013; Kango and Kumar 2016).

Initially, sand was sieved to a geometric mean size of 0.6 to 0.9 mm (This indicates that a coarse fraction of the sand was taken which passed through 0.97 mm sieve and was retained back on 0.625 mm sieve size.) soaked in an acid solution (1.0 M HCl) for 24 h, which was then washed with distilled water several times and dried at 100°C temperature. After cleaning, the sand was etched using aqua regia for 5 min and was further rinsed in a water stream to remove the etchant solution. Thereafter, the cleaned sand was dispersed in a solution containing a 2:1 ratio of $FeCl_3$ and $FeCl_2$ and to which dropwise solution of NH_4OH was added which was mixed using a magnetic stirrer at 70°C temperature for 30 min under the flow of argon (Ar).

The addition of NH_4OH led to a coprecipitation reaction and resulted in the formation of magnetite (Fe_3O_4) nanoparticles in the precursor solution. Since the sand particles were added to the precursor solution, Fe_3O_4 nanoparticles were also nucleated on the surface of the sand. The obtained mixture was cured at room temperature for 48 h and filtered and dried in a furnace at 85°C in the Ar gas environment. To ensure a proper coating of Fe_3O_4 nanoparticles on the surface of sand particles, the coated sand was washed with distilled water until a clear supernatant was obtained. Finally, the magnetite nanoparticles coated sand was stored in PVC bottles to perform batch experiments.

Batch adsorption experiments

The batch adsorption studies were performed in two phases to examine the adsorption performance of the magnetite coated nanoparticles with respect to the different operational parameters including contact time, adsorbent dose, and initial Cr(VI) concentration. In the first phase of the study, synthetic wastewater was used to evaluate the removal efficiency of Cr(VI) and different adsorption parameters. In the second phase, pharmaceutical industry wastewater was used to investigate the adsorption response of the magnetite coated sand particles, keeping all other experimental conditions and parameter specifications the same as used in the first phase of the study. The batch adsorption experiments and consequent adsorption isotherms were determined at room temperature. Other experimental conditions included maintenance of constant pH conditions of 4.0 (Zhang et al. 2020) and the use of an incubator shaker maintained at an agitation speed of 200 rpm (Kango and Kumar 2016; Islam et al. 2019).

The effect of contact time on Cr(VI) adsorption was investigated by varying the contact time from 30 to 180 min, using 25 g/L adsorbents at an initial Cr(VI) concentration of 1 mg/L. Similarly, the effect of the adsorbent dose on Cr(VI) removal was investigated by varying the adsorbent dose from 5 to 30 g/L for both synthetic and pharmaceutical wastewater keeping other parameters constant. Further, to study the adsorption isotherms, the concentration of Cr(VI) in synthetic and pharmaceutical wastewater was varied from 1 to 25 mg/L and 0.5 to 3 mg/L, respectively, for the fixed values of contact time, optimum adsorbent dose, and constant pH of 4.0.

The removal efficiency of Cr(VI) on magnetite nanoparticles coated sand adsorbent was calculated using Eq. (1), and the adsorption capacity of adsorbent for Cr(VI) (i.e., q_e) was determined using Eq. (2):

$$\%\text{Cr (VI)removal} = \frac{C_o - C_e}{C_o} \times 100 \quad (1)$$

$$q_e = \frac{C_o - C_e}{M} \times V \quad (2)$$

where C_0 is the initial Cr(VI) concentration (mg/L), C_e is the final Cr(VI) concentrations (mg/L), V is the volume of solution in liters, and M is the mass of the adsorbent in grams.

Equilibrium isotherm analysis

The isotherm model parameters often provide insights into the adsorption mechanism, the affinity, and the surface properties of the adsorbent (Yu and Neretnieks 1990; Ayawei et al. 2017). In the present study Freundlich, Langmuir, and Redlich–Peterson isotherm models were used to fit the experimental data.

The Langmuir isotherm suggests monolayer adsorption on a homogeneous surface with a limited number of active sites, and there is no interaction between adsorbed molecules on the adsorbent sites, as each active site adsorbs one molecule (Langmuir 1918). The Freundlich isotherm describes multilayer adsorption on a heterogeneous surface with an interaction between adsorbed molecules. The Redlich–Peterson equation is an empirical equation with three parameters that are used in both adsorptions on heterogeneous and homogeneous surfaces (Redlich and Peterson 1959). This isotherm is reduced to the Freundlich isotherm when the exponent is equal to 0. Moreover, when the exponent is equal to 1, this model is reduced to the two-parameter Langmuir isotherm. The mathematical equations associated with the selected nonlinear isotherm models have been summarized in Eqs. (3)–(5).

Freundlich isotherm

$$q_e = K_F C_e^{1/n} \quad (3)$$

Langmuir isotherm

$$q_e = \frac{q_m b C_e}{1 + b C_e} \quad (4)$$

Redlich–Peterson

$$q_e = \frac{A C_e}{1 + K C_e^{\beta}} \quad (5)$$

Further, nonlinear regression analysis (Tvrdik et al. 2007) was used to investigate the adsorption isotherm parameters to maximize the coefficient of determination (R^2) between the experimental data and isotherms. Additionally, statistical parameter mean standard deviation was used to determine the best fit adsorption isotherm (Manohar et al. 2006).

The rate of adsorption and rate-controlling step were determined using the pseudo-first-order and pseudo-second-order kinetic models. The pseudo-first-order kinetic model is represented by Eq. (6) (Lagergren 1898; Sathvika et al. 2016).

$$\log(q_e - q_t) = \log q_e - \frac{k_{ads} t}{2.303} \quad (6)$$

where q_e (mg/g) is the adsorption capacity at equilibrium (e) and q_t (mg/g) is the adsorption capacity at time (t). k_{ads} is the rate constant for pseudo-first-order kinetics, which can be obtained from the slope of the linear plot of log ($q_e - q_t$) versus time (t).

The pseudo-second-order kinetic model is represented by Eq. (7) (Ho and McKay 1998; Sari et al. 2008; Sathvika et al. 2016).

$$\frac{t}{q_t} = \frac{1}{h} + \frac{t}{q_e} \quad (7a)$$

where

$$h = k q_e^2 \quad (7b)$$

In the aforementioned equations, q_e (mg/g) is the amount of Cr(VI) adsorbed per unit mass of adsorbent at equilibrium (e), and q_t (mg/g) is the amount of Cr(VI) adsorbed per unit mass of adsorbent at a time (t). "h" is the initial adsorption rate (mg g^{-1} h^{-1}) and "k" is pseudo-second-order adsorption rate constant. The values of "q_e" (1/slope), "h" (1/intercept), and "k" (slope^2/intercept) can be calculated from the plots of t/q_t versus time (t).

Additionally, the secondary adsorption mechanism was also explained by using an intraparticle diffusion model. Equation (8) represents the intraparticle diffusion model (Weber Jr and Morris 1963; Sathvika et al. 2016; Sari et al. 2008).

$$q_t = k_i t^{1/2} \quad (8)$$

where k_i is intraparticle diffusion rate constant and q_t is the amount of Cr(VI) adsorbed per unit mass of adsorbent at time t. According to this model, if the graph between q_t and $t^{1/2}$ is linear then intraparticle diffusion is the rate-limiting step. Moreover, the plot should pass through the origin of intraparticle diffusion to be the sole rate-limiting step.

Results and discussion

Characterization of adsorbent

It may be noted that before coating with Fe_3O_4, the sand particles appear grayish white; and after magnetite coating, the sand particle appears black, which suggests coating of magnetite on the sand surface.

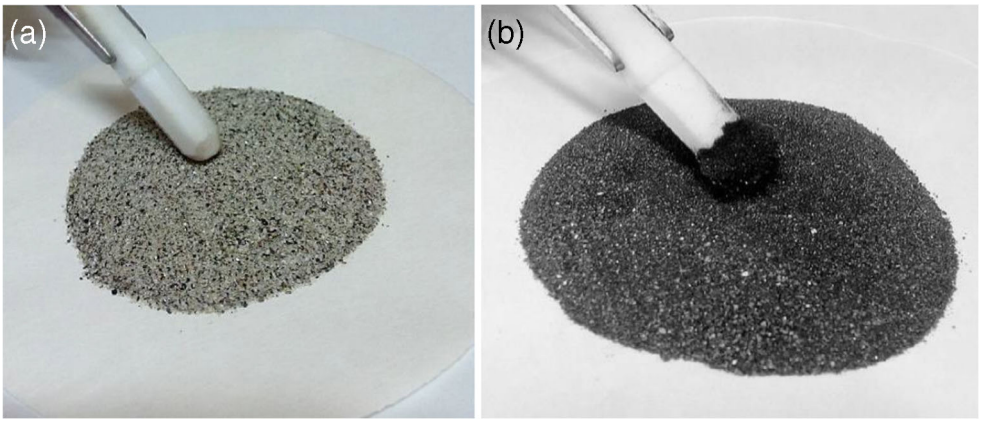

Fig. 1 The response of **a** uncoated sand and **b** magnetite coated sand particles to a magnetic bead

Figure 1a demonstrates the uncoated sand particles which are not attracted by magnetic globule. Accordingly, magnetite nanoparticles coated sand particle is attracted in by the magnetic beads, as observed in Fig. 1b, as the magnetite nanoparticles covered sand particles are attracted in by magnetic globule indicating the arrangement of magnetite nanoparticles on the sand surface.

The morphology of magnetite nanoparticles was investigated by field emission scanning electron microscopy (FESEM) (Model-Hitachi S-4700), as shown in Fig. 2. In particular, Fig. 2a, b, presents FESEM images of uncoated sand particles and magnetite coated sand particles, respectively. The FESEM images show the surface of uncoated sand particles appears as clear, while after coating, the surface of the sand is covered with Fe_3O_4 nanoparticles. The particle size distribution of the magnetite coated sand particles (Fig. 2b) was determined using the software image J and was determined to be in ranges of 30–210 nm. In principle, the magnetite coated particles vary between different size ranges, for example, 60–310 nm (Guo et al. 2016).

Effect of contact time on Cr(VI) removal

Figure 3 presents the effect of contact time on the percentage of Cr(VI) removal efficiency and adsorption capacity (q_t = mg/g) for a fixed adsorbent dose of 25 mg/L and initial Cr(VI) concentration of 1 mg/L for both synthetic and pharmaceutical wastewater.

In the first phase of the study using synthetic wastewater, removal efficiency of 85.4% of Cr(VI) was observed within the first 30 min of contact time due to rapid removal. However, the removal rate decreases after 30 min, and it takes about 120 min to attain the adsorption equilibrium. The initial rapid adsorption of Cr(VI) by Fe_3O_4 nanoparticles coated sand may be attributed to a surface adsorption process wherein all the adsorption sites, available on the outer surface of the adsorbent, are rapidly occupied by Cr(VI). This initial adsorption mechanism is known as *adsorption controlled by the surface processes* (Chowdhury and Yanful 2010). However, after 30 min, when all the immediate surface adsorption sites of the adsorbent are filled, the removal rate of Cr(VI) decreases as no immediate contact surface in the magnetite nanoparticles were available for Cr(VI). Hence, Cr(VI) present in the solution approaches the available adsorption sites of sublayered magnetite nanoparticles.

When the process of removal becomes slower, a secondary adsorption process is introduced wherein the Cr(VI) has to diffuse into the magnetite nanoparticle coating to reach the available adsorption sites (Ren et al. 2011). This secondary adsorption process is diffusion controlled and is known as *adsorption controlled by diffusion* (Ren et al. 2011) and is primarily the intraparticle diffusion of Cr(VI), which

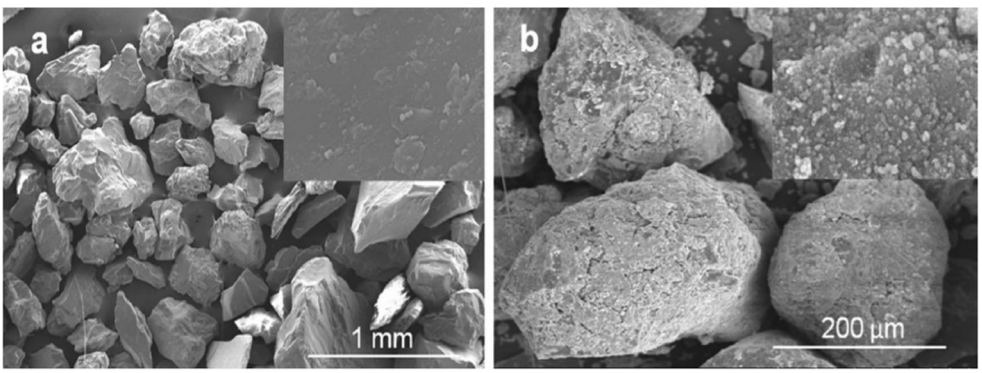

Fig. 2 FESEM images of **a** uncoated sand particles and **b** magnetite nanoparticles coated sand particles

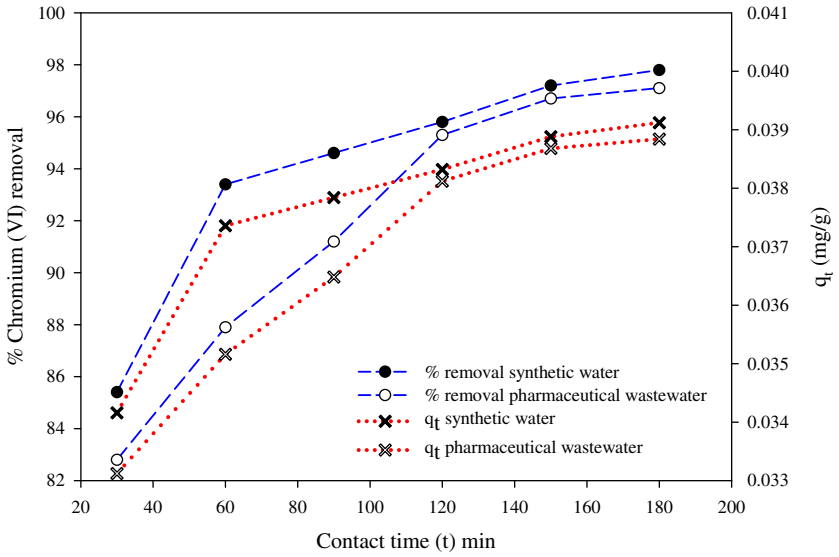

Fig. 3 Effect of contact time on % Cr(VI) removal efficiency and adsorption capacity (qe = mg/g) for synthetic and pharmaceutical wastewater (Cr(VI) concentration 1 mg/L, pH 4.0, adsorbent dose 25 g, room temperature)

decreases the rate of adsorption. The diffusion-controlled adsorption process is dependent on the intraparticle diffusion distance.

In the second phase of the study using pharmaceutical wastewater, initially, 82.8% of Cr(VI) removal takes place within 30 min of contact time due to rapid removal from pharmaceutical wastewater and takes 120 min to achieve the adsorption equilibrium. However, the removal rate of Cr(VI) for pharmaceutical wastewater was slightly lower than synthetic wastewater due to the possible presence of other adsorbates in the sample. At equilibrium conditions, almost similar removal efficiency of 97.80% and 97.10% of Cr(VI) was observed for synthetic and pharmaceutical wastewater respectively with an initial Cr(VI) concentration of 1.0 mg/L for both the samples.

Kinetic modeling

The graphical representations of pseudo-first-order and pseudo-second-order kinetic models for synthetic and pharmaceutical wastewater are shown in Fig. 4a, b, respectively. The values of kinetic model parameters including k_{ads}, k, h, and correlation coefficients (R^2) obtained from these plots are summarized in Table 1.

The experimental data matched with the pseudo-second-order kinetic model with a higher correlation coefficient (R^2 = 0.999) for both the synthetic and the industrial wastewater in comparison to the pseudo-first-order kinetic model which showed an R^2 = 0.95 and 0.973 respectively for synthetic and industrial pharmaceutical wastewater. It was further observed from Table 1 that from the normalized standard deviation values obtained for the considered kinetic modeling analysis, the pseudo-second-order model was best fitted for both the synthetic and pharmaceutical wastewater.

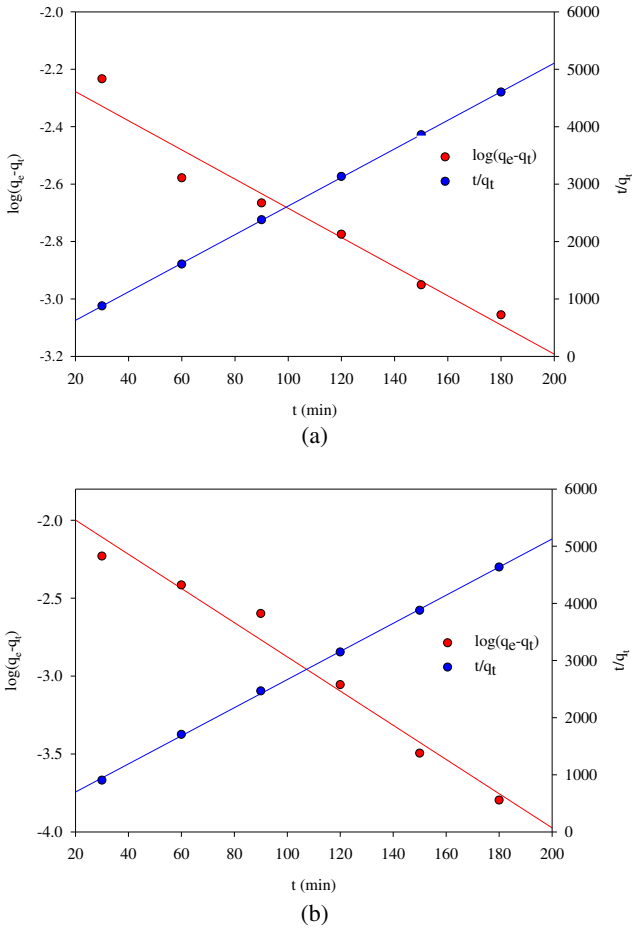

Fig. 4 Adsorption kinetics of pseudo-first-order model and pseudo-second-order model for Cr(VI) removal by Fe_3O_4 nanoparticles coated sand for **a** synthetic and **b** pharmaceutical wastewater (Cr(VI) concentration 1 mg/L, pH 4.0, adsorbent dose 25 g, room temperature)

Table 1 Pseudo-first-order and pseudo-second-order kinetic model parameters and intraparticle diffusion model parameters for Cr(VI) adsorption by Fe_3O_4 nanoparticles coated sand for synthetic and pharmaceutical wastewater

		Pseudo-first-order parameters				Pseudo-second-order parameters								Intraparticle diffusion model parameters			
Normalized standard deviation	k_{ads} (min^{-1})	Standard error for k_{ads}	R^2	Normalized standard deviation (%)	q_e (mg/g)	Standard error for q_{ei}	h (g/mg/min)	Standard error for h	q_e (mg/g)	Standard error for q_e	K (g/mg/min)	R^2	Normalized standard deviation (%)	Experimental q_e (mg/g)	K_i ($mg.g^{-1}$ $min^{1/2}$)	Standard error for K_i	R^2	Normalized standard deviation (%)
Synthetic wastewater	0.012	0.008	0.95	5.41	0.007	0.001	0.008	0.00	0.04	-*	4.81	0.999	1.33	0.039	0.001	-*	0.86	4.39
Pharmaceutical wastewater	0.025	0.002	0.973	7.84	0.016	0.002	0.005	0.001	0.04	-*	3.06	0.999	5.03	0.039	0.001	-*	0.97	3.11

* Significant digits considered up to 3 decimal places

Further, it was observed from the kinetic study that the pseudo-second-order kinetic model predicted the theoretical q_e value as 0.04 mg/g, which was almost an exact representation of the experimental q_e value of 0.0388 mg/g for the synthetic wastewater sample. For the same sample, the theoretical q_e value was determined to be 0.0066 mg/g using the pseudo-first-order kinetic model for the synthetic waste. Similarly, for pharmaceutical wastewater, the theoretical value of q_e (0.04 mg/g) obtained from the pseudo-second-order kinetic model was a better fit for experimental q_e value of 0.039 mg/g in comparison to the theoretical value of q_e of 0.016 mg/g obtained from the pseudo-first-order kinetic model.

The plots of the intraparticle diffusion model are shown in Fig. 5a, b, for synthetic and pharmaceutical wastewater, respectively. Intraparticle diffusion rate constant values obtained from these plots and the corresponding correlation coefficients (R^2) have been summarized in Table 1. It may be observed from Fig. 5 that for the present study, the plot of q_t and $t^{1/2}$ is nonlinear and the plot does not pass through the origin. It can also be observed from these figures that the adsorption mechanism is a three-phase process: (i) the initial sharper portion features boundary layer diffusion of adsorbate molecules; (ii) the second portion attributes a gradual adsorption phase, where intraparticle diffusion is the rate-limiting step, and (iii) the final equilibrium phase. However, it is also observed from Fig. 5 that for pharmaceutical wastewater in the initial phase of the experiment, the intraparticle diffusion mechanism significantly exists and the contribution from boundary layer diffusion is minor; whereas in synthetic wastewater, boundary layer diffusion mechanism predominates. This is also observed from Fig. 3 which indicates the dominance of boundary layer diffusion mechanism for synthetic wastewater as 93.4% of Cr(VI) removal was achieved within an initial 60 min of contact time.

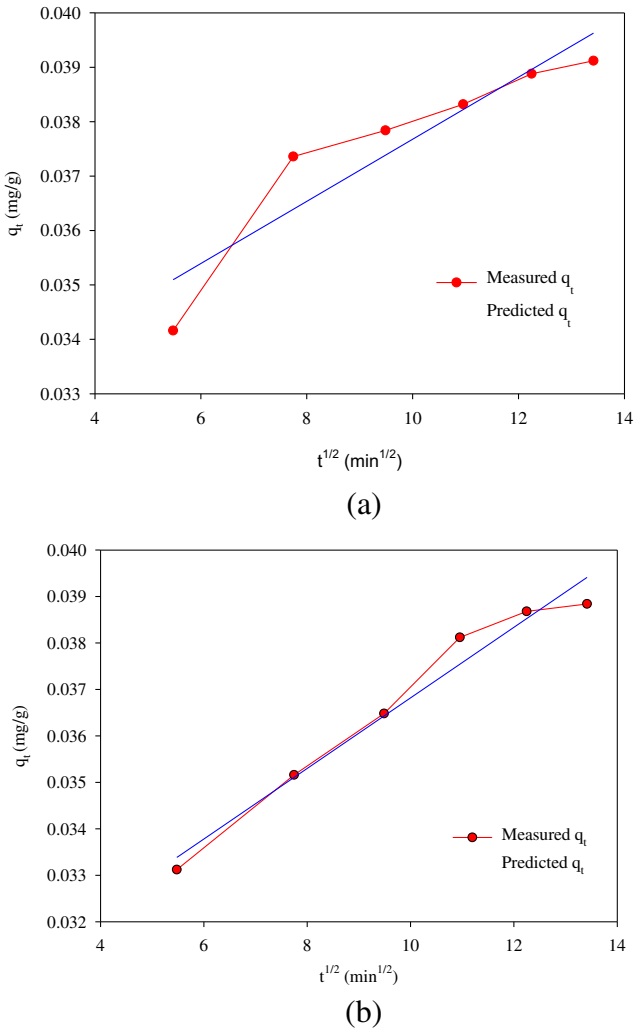

Fig. 5 Intraparticle diffusion model for Cr(VI) removal by Fe_3O_4 nanoparticles coated for **a** synthetic and **b** pharmaceutical wastewater (Cr(VI) concentration 1 mg/L, pH 4.0, adsorbent dose 25 g, room temperature)

Effect of adsorbent dose

The influence of adsorbent dose on adsorption capacity (q_e = mg/g) and Cr(VI) removal efficiency at fixed initial Cr(VI) concentration (1 mg/L) for both synthetic and pharmaceutical wastewater is shown in Fig. 6a, b, respectively. In the present study, the batch experiments were performed at pH 4.0 as has been the practice in earlier reported literature (Kango and Kumar 2016; Islam et al. 2019; Zhang et al. 2020). It can be observed that as the adsorbent dose increases from 5 to 30 g/L, the Cr(VI) removal efficiency also increases from 66.1 to 96% and 68.6 to 95.4% for synthetic and pharmaceutical wastewater, respectively. The increase in removal efficiency was due to the more available adsorption sites at higher concentrations of the adsorbent (Pandey et al. 2009; Kaczala et al. 2009).

It was also observed from these figures that an increase of adsorbent dose beyond 25 g/L, showed no significant change in removal efficiency of Cr(VI). Further, at this adsorbent dose, all the Cr(VI) ion concentration had already been adsorbed for both the samples, and an increase in the adsorbent dose led to the availability of additional free active adsorption sites (increased availability of active binding sites) which could adsorb more of Cr(VI) concentration if it were available in the samples.

However, the adsorption capacity decreases with an additional increase in the adsorbent dose. The adsorption capacity decreased from 0.132 to 0.032 mg/g for synthetic wastewater and 0.137 to 0.032 mg/g for pharmaceutical wastewater over the range of adsorbent doses studied. The interaction between adsorbent molecules is a significant factor in the adsorption process, with a higher amount of adsorbate being adsorbed when the distance between the adsorbent molecules is greater (Itoh et al. 1975). Hence, the decrease in adsorption capacity is possibly due to the interference between binding sites at higher adsorbent dose or an inadequate number of available

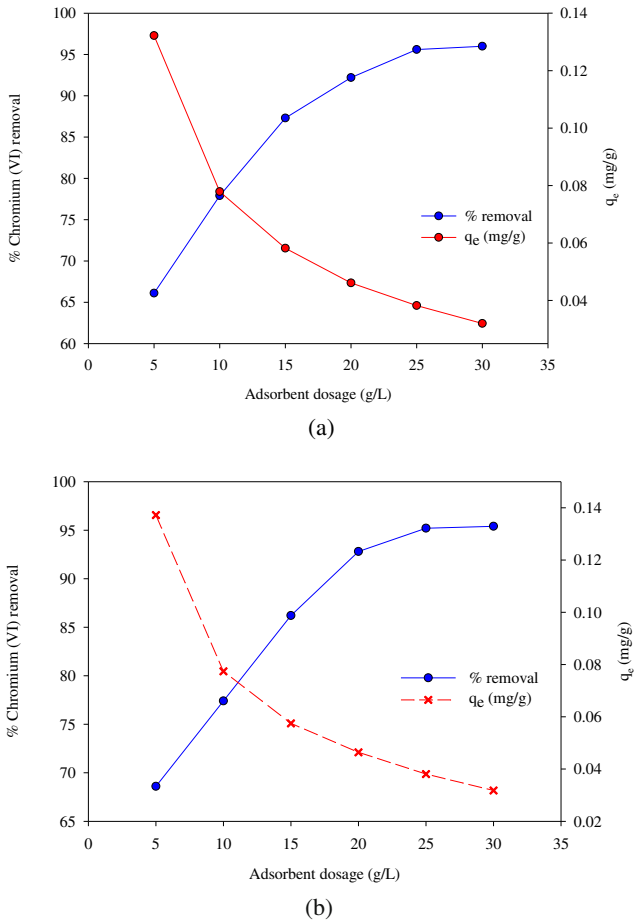

Fig. 6 Effect of adsorbent dose on % Cr(VI) removal efficiency and adsorption capacity (qe = mg/g) for **a** synthetic and **b** pharmaceutical wastewater (Cr(VI) concentration 1 mg/L, pH 4.0, room temperature)

Cr ions in the wastewater when compared to available binding sites on the adsorbent (Fan et al. 2008; Rome and Gadd 1987; Chen et al. 2011). Further, in Fig. 6a, b, the point of intersection between removal efficiency and adsorbent capacity is usually considered as the optimum dose which represents the optimal balance between Cr(VI) removal efficiency and adsorption capacity (Kango and Kumar 2016). In the present study, this was determined to be 10.36 g/L and 11 g/L of adsorbent dose for synthetic and pharmaceutical wastewater, respectively, from the subsequent graphs. Further, for the abovementioned adsorbent dose, only 77.9% and 80.2% Cr(VI) removal was recorded for synthetic and pharmaceutical wastewater, respectively.

Effect of initial Cr(VI) concentration

The effect of initial Cr(VI) concentration on the removal efficiency and adsorption capacity (q_e) of Fe_3O_4 nanoparticles coated sand is shown in Fig. 7a, b, for synthetic and pharmaceutical wastewater, respectively. It was observed that the Cr(VI) removal efficiency decreased with an increase in the initial Cr(VI) concentration, while the adsorption capacity (q_e) increased. This is primarily because of a sufficiently large number of active sites on the adsorbent surface at lower Cr(VI) concentration which can easily accommodate all of the Cr(VI) ions. An increase in Cr(VI) concentration induces a decrease in the availability of the surface active sites leading to a decrease in the removal efficiency of Cr(VI) due to an insufficient accommodation of Cr(VI) ions. In addition, initial Cr(VI) concentration provides a driving force to overcome all mass transfer resistances between the adsorbent and adsorption medium resulting in higher adsorption capacities at higher initial Cr(VI) concentration (Fan et al. 2008). The dependence of adsorption on Cr(VI) concentration at equilibrium was investigated and modeled using different isotherm models which have been presented in the next section.

Adsorption isotherms

The adsorption isotherms are useful in understanding the adsorption process and demonstrate adsorbate and adsorbent interaction in an adsorption system. Though different adsorption isotherm models are available to investigate experimental equilibrium parameters, Freundlich and Langmuir isotherms are the most widely used for the application in water and wastewater treatment (Wu et al. 2009). In the present study,

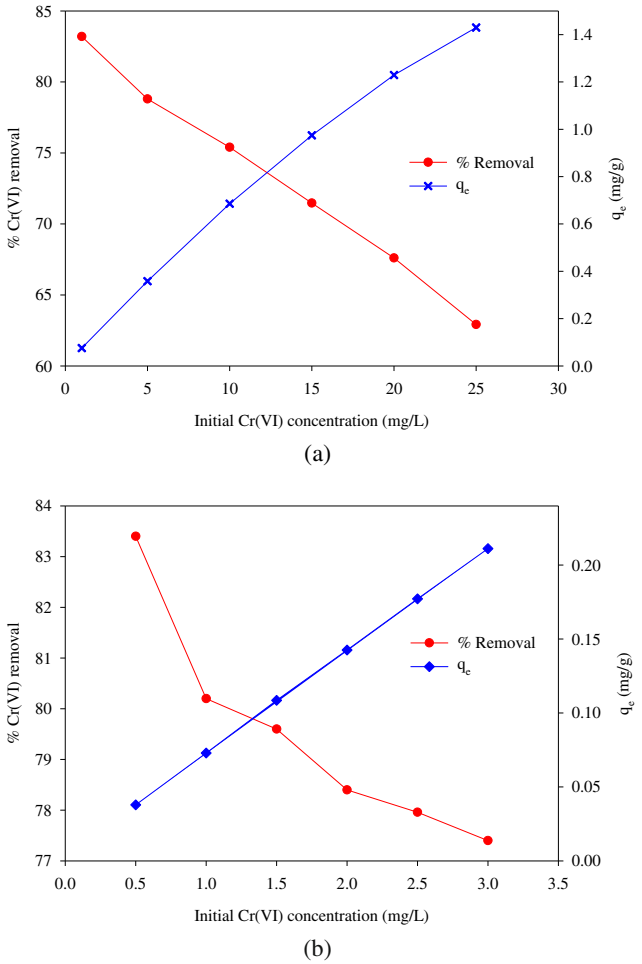

Fig. 7 Effect of initial Cr(VI) concentration on % Cr(VI) removal efficiency and adsorption capacity (qe = mg/g) for **a** synthetic wastewater and **b** pharmaceutical wastewater (pH 4.0, adsorbent dose 11 g, room temperature)

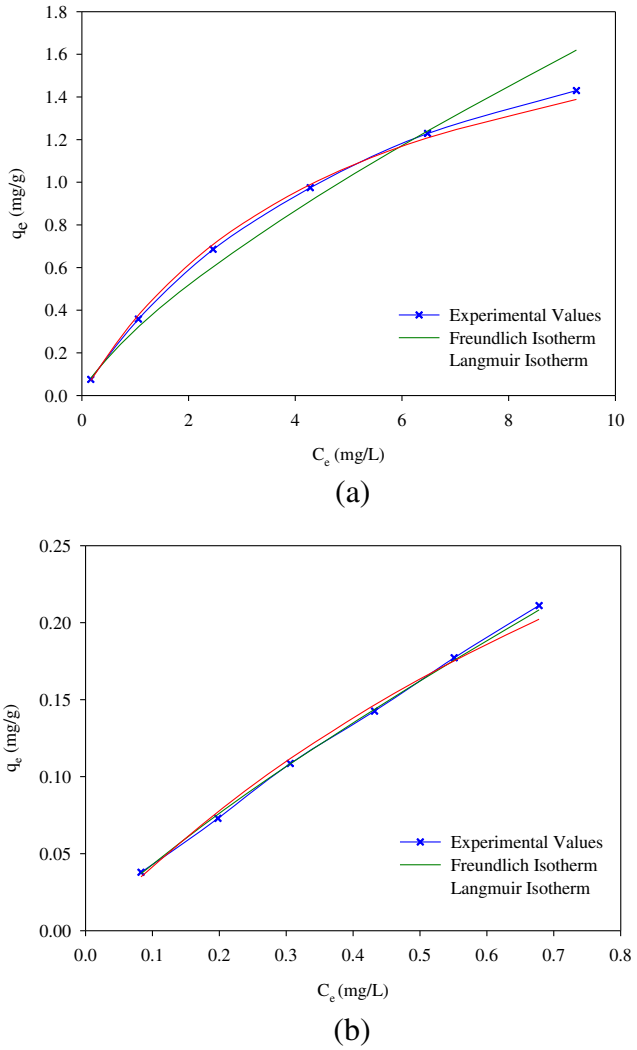

Fig. 8 Adsorption isotherm, Freundlich and Langmuir for Cr(VI) adsorption by Fe_3O_4 nanoparticles coated sand from **a** synthetic wastewater and **b** pharmaceutical wastewater

nonlinear isotherm models (Freundlich, Langmuir, and Redlich–Peterson isotherms) were used to investigate the different adsorption equilibrium parameters and to study the adsorbate–adsorbent interaction.

It can be observed from Figs. 8 and 9 that for synthetic wastewater, the nonlinear Langmuir and Redlich–Peterson isotherm models present higher R^2 value than the Freundlich model, indicating them to be a better fit for the experimental studies conducted. In agreement, the Redlich–Peterson model showed a strong relationship for Cr(VI) adsorption in synthetic wastewater at room temperature. Conversely, the Freundlich model adjustment was observed to be a better fit for Cr(VI) on magnetite for pharmaceutical wastewater (Fig. 8b) with a correlation coefficient of 0.999.

Comparing the R^2 values obtained for each of the considered isotherms for synthetic wastewater, the best fit follows the sequence wherein the Redlich–Peterson was determined to be the best followed by Langmuir and Freundlich isotherms. Similarly, for pharmaceutical waste, the best fit sequence was observed for Redlich–Peterson followed by Freundlich and Langmuir isotherms.

However, it was interesting to note that a Langmuir-like "plateau progression" trend was observed in the Freundlich fit (Fig. 8a) instead of the typical "exponential progression" which implies monolayer adsorption. Further, the Freundlich coefficient value ($n = 1.21 < 2$) also suggests an erratic fit of the model equation. Hence, it may be mentioned that even though the R^2 value obtained from the Freundlich isotherm may be on the higher side, the visual representations of the graphical plots are erratic in nature as they do not show an exponential trend. Hence, the use of the Freundlich equation simply on the basis of the R^2 value may lead to faulty conclusions regarding the behavior between the adsorbent and the adsorbate. It was further observed from Table 2 that from the normalized standard deviation values obtained for the considered isotherms, the Redlich–Peterson equation was best fitted for both the synthetic and pharmaceutical wastewater.

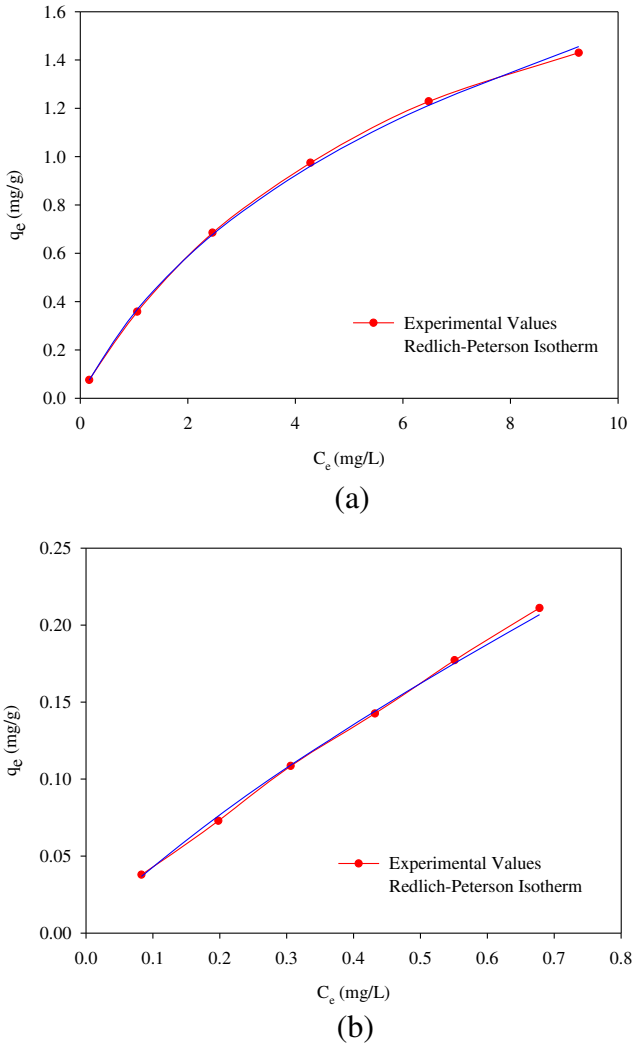

Fig. 9 Redlich–Peterson isotherm, **a** synthetic wastewater and **b** pharmaceutical wastewater for Cr(VI) adsorption by Fe_3O_4 nanoparticles coated sand

Finally, it may be summarized that the adsorption data were best fitted by the Redlich–Peterson isotherm model for both synthetic and pharmaceutical wastewater. Furthermore, the higher values of Redlich–Peterson exponents (β) as shown in Table 2 suggest that Langmuir isotherm is more predominant for both synthetic and pharmaceutical wastewater. It can be interpreted from the adsorption isotherm models that the synthetic and the pharmaceutical wastewater follow the chemisorption process over physical adsorption. This is because when comparing the exponent of the Redlich–Peterson isotherm, it was observed that the value was 0.76 (close to 1) which indicates that it follows the Langmuir process. Additionally, Langmuir fit basically signifies the chemisorptions process as reported in earlier scientific literature, and hence, chemisorption is the method via which the adsorption process takes place (Tran et al. 2017). Finally, for our study, the Freundlich isotherm did not fit the experimental

Table 2 Adsorption isotherm parameters for Cr(VI) removal by Fe_3O_4 nanoparticles coated sand

Nonlinear adsorption models																				
	Freundlich isotherm					Langmuir isotherm					Redlich–Peterson isotherm									
	K_F	Standard error for K_F	n	Standard error for n	R^2	Normalized standard deviation (%)	b	Standard error for b	q_m	Standard error for q_m	R^2	Normalized standard deviation (%)	A	Standard error for A	K	Standard error for K	β	Standard error for β	R^2	Normalized standard deviation (%)
Synthetic	0.31	0.026	1.35	0.010	0.979	22.79	0.20	0.004	2.12	0.029	0.998	9.82	0.49	0.030	0.39	0.053	0.76	0.037	0.999	4.20
Pharmaceutical	0.29	0.002	1.21	0.015	0.999	9.70	0.61	0.850	0.73	0.138	0.994	11.04	0.99	0.003	0.41	0.058	0.87	0.004	0.999	9.03

* Significant digits considered up to 3 decimal places

Table 3 Comparison of adsorption capacities of different low-cost adsorbent for Cr(VI) removal

Low-cost adsorbents	Experimental conditions	Langmuir adsorption capacity (q_m) (mg/g)	References
Dolochar	Initial Cr(VI) concentration 50 mg/L, temperature 30°C, adsorbent dose 20 g, pH 2.0	0.904	Panda et al. (2017)
Chemically modified banana peels	Initial Cr(VI) concentration 100 mg/L, pH 3.0, adsorbent dose 1 g, temperature 30°C, pH 3.0	6.16	Ali et al. (2016b)
Hibiscus Cannabinus kenaf	Initial Cr(VI) concentration 0.5–10 mg/L, adsorbent dose 2 g, temperature 23 ± 2°C, pH 7.0	0.52	Borna et al. (2016)
Greensand (glauconite)	Initial Cr(VI) concentration 0.2–10 mg/L, adsorbent dose 1 g, temperature 25°C, pH 7.0	12.21	Naghipour et al. (2020)
Red mud	Initial Cr(VI) concentration 192.308 and 576.923 μmol/L, adsorbent dose 3 g, temperature 25°C, pH 5–7	0.496	Tsamo et al. (2018)
Sawdust	Initial Cr(VI) concentration 5 to 100 mg/L, adsorbent dose 20 g, temperature 25°C	4.44	Gupta et al. (2009)
Charcoal	Initial Cr(VI) concentration 20 and 1000 mg/L, adsorbent dose 80 g, temperature 30°C	6.78	Gupta et al. (2009)
Fe3O4@NiO core-shell nanocomposite	Initial Cr(VI) concentration 6 and 67 mg/L, adsorbent dose 0.6 g, temperature 25°C	6.88	Mahmoudi and Behnajady (2018)
Copper slag@polyaniline composite	Initial Cr(VI) concentration 100 and 300 mg/L, adsorbent dose 0.01 g, temperature 50°C, pH 2	452.54	Wu et al. (2021)
Magnetite	Initial Cr(VI) concentration 1–25 mg/L, adsorbent dose 11 g, room temperature, pH 4.0	2.12	Present study

conditions; and as reported in earlier scientific studies, the Freundlich isotherm fit generally signifies the physical adsorption process.

In general, the adsorption of Cr(VI) is possible because of the reduction of highly oxidizable Cr(VI) to Cr(III) cations due to the possible formation of chelate on the adsorbent surface (Wu et al. 2021). Accordingly, the better performance of the pseudo-second-order kinetic model indicates good agreement with chemisorptions (Panda et al. 2017).

Adsorption efficiency

A dimensionless quantity "r" was calculated to analyze the adsorption efficiency of the method by using the subsequent equation (Eq. 9) (Kango and Kumar 2016).

$$r = \frac{1}{1 + bC_0} \tag{9}$$

where C_0 is the initial Cr(VI) concentration and "b" is the Langmuir isotherm constant. An "r" value of less than 1.0 signifies favorable adsorption conditions, whereas "r" values greater than 1.0 are deemed unfavorable. The associated parameters of the mentioned isotherm models are listed in Table 2.

In the present study, the adsorption efficiency for both synthetic wastewater (r = 0.83) and pharmaceutical wastewater (r = 0.62) was less than 1 with a reducing order at high Cr(VI) concentrations, indicating highly favorable adsorption of Cr(VI) on magnetite nanoparticles coated sand. The Freundlich exponent (n) is obtained as 1.35 and 1.21 for synthetic and pharmaceutical wastewater, respectively. Additionally, it has been reported that n values satisfying the conditions (1/n < 1.0) are favorable for adsorption of Cr(VI) on magnetite nanoparticles (Hu et al. 2004). For our studies, the corresponding values of 1/n were determined to be 0.74 and 0.83 for synthetic and industrial wastes, respectively. The maximum adsorption capacity (q_e) for Cr(VI) removal is obtained at 2.12 mg/g, which is comparable with other reported adsorbents (Panda et al. 2017). The comparison of the Langmuir adsorption model for adsorption capacity of low-cost adsorbents for Cr(VI) removal with reported is given in Table 3.

Limitations of the study

Due to the nonpreservance of the experimental samples, the authors were not able to further extend the time study beyond 180 min and report it in the present study. Additionally, the considered formed magnetic phase is magnetite, although it was not confirmed by the used experimental techniques. Hence, these may be considered as specific limitations of the study.

Conclusion

The major conclusions obtained from the study are summarized as follows:

- The removal efficiency of Cr(VI) was found to be 85.4% and 82.8% respectively for synthetic and pharmaceutical wastewater for a contact time of 30 min with experimental conditions of pH of 4.0, room temperature (25 + 3°C), and initial Cr(VI) concentration of 1 mg/L for both and adsorbent dose of 25 mg/L. It may be concluded from the study that magnetite nanoparticles coated on the sand (a low-cost adsorbent) can be used effectively for Cr(VI) removal from synthetic and pharmaceutical wastewater.
- The experimental data were best fitted by the pseudo-second-order kinetic model (R^2 = 0.999; normalized standard deviation of 1.33 and 5.03 for synthetic and pharmaceutical wastes, respectively) for both the types of wastewater used in the study. It may be concluded from the previous context that the chemisorption process is the major driving force of the adsorption mechanism.
- The adsorbate dose determined using the pseudo-second-order kinetic model (q_e of 0.04 mg/g) was similar to the actual experiment (q_e of 0.0388 mg/g) for the synthetic wastewater sample. Hence, it may be concluded that there was a high level of agreement between the adsorbent dosages determined experimentally and using the pseudo-second-order kinetic model.
- The maximum adsorbate dose was determined to be 25 g/L (for maximum removal efficiency) with the optimum dose of adsorbate being designed as 10.36 and 11.0 g/L with removal efficiencies of 77.9% and 80.2% for synthetic and pharmaceutical wastes, respectively. Further, with an increase in adsorbent dose, a decrease in removal efficiency was reported. It may be concluded from this that the process of decrease in removal efficiency with increased adsorbent dose may be attributed to the interference between binding sites at a higher adsorbent dose as has been reported in earlier scientific literature.
- It may be concluded from the adsorption studies that Redlich–Peterson isotherms were the best fit for both synthetic and pharmaceutical wastes, respectively.
- Further, for the experimental study conditions, the Langmuir isotherm also was well fitted which suggests a monolayer chemisorption process on a homogeneous adsorbent surface and as also supported by the results obtained from the pseudo-second-order kinetic model.
- It may be concluded from the study that the use of magnetite coated sand is highly suitable for removal of Cr(VI) concentrations as observed for both synthetic and pharmaceutical wastewater since the determined values for a parameter (r) were less than 1.
- In an overall sense, it may be concluded that magnetite coated sand used as a low-cost adsorbent is highly efficient and well suited for the removal of heavy metals and in particular Cr(VI). Further, the adsorbent itself acts as a filter cartridge without the need for an external magnetic separation that renders the process highly environmentally friendly.

Acknowledgements The authors take this opportunity in thanking the distinguished reviewers and the editor for their incisive comments which led to a huge improvement in the quality of the research paper.

Author contribution SL conducted the initial experiments including the preparation of the adsorbent and reported the results and prepared the initial manuscript. AD examined the data, did the kinetic modeling, and reviewed the initial manuscript. RG was involved in the conceptualization of the study and reviewing the results and was also involved in the overall supervision of the study.

Data Availability All data generated or analyzed during this study are included in this published article.

Declarations

Ethics approval and consent to participate Not applicable.

Consent for publication Not applicable.

Conflict of interest The authors declare that they have no competing interests.

References

Ali A, Hira Zafar MZ, Ul Haq I, Phull AR, Ali JS, Hussain A (2016a) Synthesis, characterization, applications, and challenges of iron oxide nanoparticles. Nanotechnol Sci Appl 9:49

Ali A, Saeed K, Mabood F (2016b) Removal of chromium (VI) from aqueous medium using chemically modified banana peels as efficient low-cost adsorbent. Alex Eng J 55(3):2933–2942

Ali H, Khan E, Ilahi I (2019) Ehazardous heavy metals: environmental persistence, toxicity, and bioaccumulation. J Chem art. no. 6730305

Ayawei N, Ebelegi AN, Wankasi D (2017) Modelling and interpretation of adsorption isotherms. J Chem art. no. 3039817

Borna MO, Pirsaheb M, Niri MV, Mashizie RK, Kakavandi B, Zare MR, Asadi A (2016) Batch and column studies for the adsorption of chromium (VI) on low-cost Hibiscus Cannabinus kenaf, a green adsorbent. J Taiwan Inst Chem Eng 68:80–89

Chen CY, Yang CY, Chen AH (2011) Biosorption of Cu (II), Zn (II), Ni (II) and Pb (II) ions by cross-linked metal-imprinted chitosans with epichlorohydrin. J Environ Manag 92(3):796–802

Chowdhury SR, Yanful EK (2010) Arsenic and Cr removal by mixed magnetite–maghemite nanoparticles and the effect of phosphate on removal. J Environ Manag 91(11):2238–2247

CPCB (Central Pollution Control Board New Delhi) (2017) General standards for discharge of environmental pollutants part-a: effluents. New Delhi

Dave PN, Chopda LV (2014) Application of iron oxide nanomaterials for the removal of heavy metals. J Nanotechnol art. no. 398569

Fan T, Liu Y, Feng B, Zeng G, Yang C, Zhou M, Zhou H, Tan Z, Wang X (2008) Biosorption of cadmium(II), zinc(II) and lead(II) by Penicillium simplicissimum: isotherms, kinetics and thermodynamics. J Hazard Mater 160(2-3):655–661

Guo X, Wu Z, Li W, Wang Z, Li Q, Kong F, Zhang H, Zhu X, du YP, Jin Y, du Y, You J (2016) Appropriate size of magnetic nanoparticles for various bioapplications in cancer diagnostics and therapy. ACS Appl Mater Interfaces 8(5):3092–3106

Gupta VK, Carrott PJM, Carrott R, Suhas MML (2009) Low-cost adsorbents: growing approach to wastewater treatment—a review. Crit Rev Environ Sci Technol 39:783–842

Gupta A, Mohammed Y, Sankararmakrishnan N (2013) Chitosan- and iron- chitosan-coated sand filters: a cost-effective approach for enhanced arsenic removal. Ind Eng Chem Res 52(5):2066–2072

Ho YS, McKay G (1998) Kinetic models for the sorption of dye from aqueous solution by wood. J Environ Sci Health B Process Saf Environ Prot 76(2):183–191

Hu J, Lo IMC, Chen G (2004) Removal of Cr (VI) by magnetite. Water Sci Technol 50(12):139–146

Hu J, Chen G, Lo IM (2005) Removal and recovery of Cr (VI) from wastewater by maghemite nanoparticles. Water Res 39(18):4528–4536

Hu J, Chen G, Lo IM (2006) Selective removal of heavy metals from industrial wastewater using maghemite nanoparticle: performance and mechanisms. J Environ Eng 132(7):709–715

Islam MA, Angove MJ, Morton DW (2019) Recent innovative research on Cr (VI) adsorption mechanism. Environ Nanotechnol Monit Manag 12:100267

Itoh M, Yuasa M, Kobayashi T (1975) Adsorption of metal ions on yeast cells at varied cell concentrations. Plant Cell Physiol 16(6):1167–1169

Izuru S, Toshiro T, Masaru K (1976) Method of extracting heavy metals from industrial waste waters. U.S. Patent Jan. 6, 1976 3,931,007

Jaishankar M, Tseten T, Anbalagan N, Mathew BB, Beeregowda KN (2014) Toxicity, mechanism and health effects of some heavy metals. Interdiscip Toxicol 7(2):60–72

Kaczala F, Marques M, Hogland W (2009) Lead and vanadium removal from a real industrial wastewater by gravitational settling/sedimentation and sorption onto Pinus sylvestris sawdust. Bioresour Technol 100(1):235–243

Kango S, Kumar R (2016) Low-cost magnetic adsorbent for As (III) removal from water: adsorption kinetics and isotherms. Environ Monit Assess 188(1):60

Lagergren S (1898) About the theory of so-called adsorption of soluble substance. Kungliga Svenska Vetenskapsakademiens Handlingar 24:1–39

Langmuir I (1918) The adsorption of gases on plane surfaces of glass, mica and platinum. J Am Chem Soc 40(9):1361–1403

Mahmoudi E, Behnajady MA (2018) Synthesis of Fe3O4@ NiO core-shell nanocomposite by the precipitation method and investigation of Cr (VI) adsorption efficiency. Colloids Surf A Physicochem Eng Asp 538:287–296

Manohar DM, Noeline BF, Anirudhan TS (2006) Adsorption performance of Al-pillared bentonite clay for the removal of cobalt (II) from aqueous phase. Appl Clay Sci 31(3-4):194–206

Mishra S, Bharagava RN, More N, Yadav A, Zainith S, Mani S, Chowdhary P (2019) Heavy metal contamination: an alarming threat to environment and human health. In: Environmental biotechnology: for sustainable future. Springer, Singapore, pp 103–125

Naghipour D, Taghavi K, Ashournia M, Jaafari J, andArjmandMovarrekh, R. (2020) A study of Cr (VI) and NH4+ adsorption using greensand (glauconite) as a low-cost adsorbent from aqueous solutions. Water Environ J 34(1):45–56

Panda H, Tiadi N, Mohanty M, Mohanty CR (2017) Studies on adsorption behavior of an industrial waste for removal of chromium from aqueous solution. S Afr J Chem Eng 23:132–138

Pandey PK, Choubey S, Verma Y, Pandey M, Chandrashekhar K (2009) Biosorptive removal of arsenic from drinking water. Bioresour Technol 100(2):634–637

Peng H, Guo J (2020) Removal of chromium from wastewater by membrane filtration, chemical precipitation, ion exchange, adsorption electrocoagulation, electrochemical reduction, electrodialysis, electrodeionization, photocatalysis and nanotechnology: a review. Environ Chem Lett 18:2055–2068

Redlich OJDL, Peterson DL (1959) A useful adsorption isotherm. J Phys Chem 63(6):1024–1024

Ren Z, Zhang G, Chen JP (2011) Adsorptive removal of arsenic from water by an iron-zirconium binary oxide adsorbent. J Colloid Interface Sci 358(1):230–237

Rome L, Gadd GM (1987) Copper adsorption by Rhizopus arrhizus, Cladosoriumresinae and Penicillium italicum. Appl Microbiol Biotechnol 26(1):84–90

Saha R, Nandi R, Saha B (2011) Sources and toxicity of hexavalent Cr. J Coord Chem 64(10):1782–1806

Sall ML, Diaw AKD, Gningue-Sall D, Aaron SE, Aaron JJ (2020) Toxic heavy metals: impact on the environment and human health, and treatment with conducting organic polymers, a review. Environ Sci Pollut Res Int 27:29927–29942

Sari A, Mendil D, Tuzen M, Soylak M (2008) Biosorption of Cd(II) and Cr(III) from aqueous solution by moss (Hylocomium splendens) biomass: equilibrium, kinetic and thermodynamic studies. Chem Eng J 144:1–9

Sathvika T, Manasi, Rajesh V, Rajesh N (2016) Adsorption of Cr supported with various column modelling studies through the synergistic influence of Aspergillus and cellulose. J Environ Chem Eng 4:3193–3204

Shen H, Pan S, Zhang Y, Huang X, Gong H (2012) A new insight on the adsorption mechanism of amino-functionalized nano-Fe_3O_4 magnetic polymers in Cu (II), Cr (VI) co-existing water system. Chem Eng J 183:180–191

Singh J, Kalamdhad AS (2011) Effects of heavy metals on soil, plants, human health and aquatic life. Int J Res Chem Environ 1(2):15–21

Tang L, Deng S, Tan D, Long J, Lei M (2019) Heavy metal distribution, translocation, and human health risk assessment in the soil-rice system around Dongting Lake area, China. Environ Sci Pollut Res 26(17):17655–17665

Tchounwou PB, Yedjou CG, Patlolla AK, Sutton DJ (2012) Heavy metal toxicity and the environment. In: Molecular, Clinical and Environmental Toxicology. Springer, Basel, pp 133–164

Tran HN, You SJ, Hosseini-Bandegharaei A, Chao HP (2017) Mistakes and inconsistencies regarding adsorption of contaminants from aqueous solutions: a critical review. Water Res 120:88–116

Tsamo C, Djonga PD, Dikdim JD, Kamga R (2018) Kinetic and equilibrium studies of Cr (VI), Cu (II) and Pb (II) removal from aqueous solution using red mud, a low-cost adsorbent. Arab J Sci Eng 43(5):2353–2368

Tvrdík J, Křivý I, andMišík, L. (2007) Adaptive population-based search: application to estimation of nonlinear regression parameters. Comput Stat Data Anal 52(2):713–724

Ullah R, Ahmad W, Ahmad I, Khan M, Iqbal Khattak M, Hussain F (2020) Adsorption and recovery of hexavalent chromium from tannery wastewater over magnetic max phase composite. Sep Sci Technol 56(3):439–452

Weber WJ Jr, Morris JC (1963) Kinetics of adsorption oncarbon from solution, Journal of Sanitation Engineering, Division of American Society Civil Engineering. 89:31–60

Wu FC, Tseng RL, Juang RS (2009) Initial behavior of intraparticle diffusion model used in the description of kineticsadsorptionisotherms. Chem Eng J 153(1):1–8

Wu Y, Li H, Zhao Z, Yi X, Deng D, Zheng L, Luo X, Cai Y, Luo W, Zhang M (2021) Low-cost and high-efficiency metallurgical copper slag@ polyaniline core–shell composite as an adsorbent for the

removal of Cr (VI) from aqueous solution. J Alloys Compd 851: 156741

Yao B, Liu M, Gao Y, Liu Y, Cong S, Zou D (2020) Removal of hexavalent Cr in aqueous solution using organic iron-based composites synthesized and immobilized by natural dried willow leaves. J Clean Prod 247:119132

Yi Y, Tu G, Zhao D, Tsang PE, Fang Z (2020) Key role of FeO in the reduction of Cr (VI) by magnetic biochar synthesised using steel pickling waste liquor and sugarcane bagasse. J Clean Prod 245: 118886

Yu J-W, Neretnieks I (1990) Single-component and multicomponent adsorption equilibria on activated carbon of methylcyclohexane, toluene and isobutyl methyl ketone. Ind Eng Chem Res 29:220–231

Yuan P, Liu D, Fan M, Yang D, Zhu R, Ge F, He H (2010) Removal of hexavalent Cr [Cr (VI)] from aqueous solutions by the diatomite-supported/unsupported magnetite nanoparticles. J Hazard Mater 173(1-3):614–621

Zhang J, Lin S, Han M, Su Q, Xia L, Hui Z (2020) Adsorption properties of magnetic magnetite nanoparticle for coexistent Cr (VI) and Cu (II) in mixed solution. Water 12(2):446